

# Numerical simulation of the three-dimensional Rayleigh–Taylor instability



Hyun Geun Lee<sup>a</sup>, Junseok Kim<sup>b,\*</sup>

<sup>a</sup> Institute of Mathematical Sciences, Ewha W. University, Seoul 120-750, Republic of Korea

<sup>b</sup> Department of Mathematics, Korea University, Seoul 136-713, Republic of Korea

## ARTICLE INFO

### Article history:

Received 28 August 2012

Received in revised form 7 March 2013

Accepted 17 August 2013

### Keywords:

Rayleigh–Taylor instability

Phase-field method

Projection method

Time-dependent pressure boundary condition

## ABSTRACT

The Rayleigh–Taylor instability is a fundamental instability of an interface between two fluids of different densities, which occurs when the light fluid is pushing the heavy fluid. During the nonlinear stages, the growth of the Rayleigh–Taylor instability is greatly affected by three-dimensional effects. To investigate three-dimensional effects on the Rayleigh–Taylor instability, we introduce a new method of computation of the flow of two incompressible and immiscible fluids and implement a time-dependent pressure boundary condition that relates to a time-dependent density field at the domain boundary. Through numerical examples, we observe the two-layer roll-up phenomenon of the heavy fluid, which does not occur in the two-dimensional case. And by studying the positions of the bubble front, spike tip, and saddle point, we show that the three-dimensional Rayleigh–Taylor instability exhibits a stronger dependence on the density ratio than on the Reynolds number. Finally, we perform a long time three-dimensional simulation resulting in an equilibrium state.

© 2013 Elsevier Ltd. All rights reserved.

## 1. Introduction

The Rayleigh–Taylor instability (RTI) is a fundamental instability of an interface between two fluids of different densities, which occurs when a heavy fluid is superposed over a light fluid in a gravitational field or when a hydrodynamic instability occurs in any accelerating fluid system in which the density and pressure gradients have opposite signs. For a fluid in a gravitational field, the RTI was first introduced by Rayleigh [1] and later applied in considering all accelerated fluids by Taylor [2]. The Rayleigh–Taylor instability has been applied in considering a wide range of problems such as inertial confinement fusion [3–6], supernova explosion [7,8] and remnants [9,10], atmospheric physics [11], geophysics [12], and oceanography [13].

The growth of the RTI can be roughly divided into four stages [14]. In the first stage, the amplitude  $h$  of the perturbation is much smaller than the wavelength  $\lambda$ . The linear stability theory is valid and shows that the amplitude grows exponentially with time [2]:

$$h = h_0 e^{\alpha t},$$

where  $h_0$  is the initial amplitude,  $\alpha$  is the growth rate, and  $t$  is the time. The growth rate depends on the density ratio ( $\rho_H/\rho_L$ , or Atwood number  $At = (\rho_H - \rho_L)/(\rho_H + \rho_L)$ , where  $\rho_H$  and  $\rho_L$  are the densities of the heavy and light fluids, respectively), the surface tension, the viscosity, and the compressibility [14]. When the amplitude grows to a size of order  $0.1\lambda$  to  $0.4\lambda$ , substantial deviations from the linear theory are observed and the RTI evolves into the second (nonlinear) stage. During the

\* Corresponding author. Tel.: +82 2 3290 3077; fax: +82 2 929 8562.

E-mail address: [cfdkim@korea.ac.kr](mailto:cfdkim@korea.ac.kr) (J. Kim).

URL: <http://math.korea.ac.kr/~cfdkim/> (J. Kim).

second stage, the light fluid rises into the heavy fluid in the form of bubbles and the heavy fluid falls into the light fluid in the form of spikes. In the third stage, the nonlinearity becomes much stronger. The Kelvin–Helmholtz instability [15] occurs due to a velocity difference across the interface between two fluids and a roll-up of vortices forms a mushroom-type shape of the spikes. Also, there is bubble amalgamation, in which large bubbles absorb smaller ones and large bubbles grow larger and move faster. In the final stage, the RTI evolves into turbulent or chaotic mixing.

The first two stages can be dealt with by the analytic and quasi-analytic methods [15]. The behavior during the late stages is mainly studied numerically. Although there have been many numerical studies [16–26], the nonlinear evolution of the three-dimensional RTI in the late stages, which results from different dimensionless parameters or Atwood numbers, has not been well documented and, furthermore, to the best of the authors' knowledge, numerical simulations were stopped well before the fluid system reached an equilibrium state. The purpose of this paper is to investigate the late stage evolution of the three-dimensional RTI of two fluids and to perform a long time three-dimensional simulation resulting in an equilibrium state.

In this paper, direct numerical simulations of the three-dimensional RTI are carried out using a phase-field method. The main idea of the method is to treat the interface between two fluids as a thin mixing layer across which physical properties vary steeply but continuously. The method avoids a direct tracking of the interface and produces the correct interfacial tension from the mixing layer free energy. The properties and evolution of the mixing layer are governed by an order parameter  $\phi$  (a phase-field variable) that obeys the Cahn–Hilliard equation [27]. The Cahn–Hilliard equation has been extensively studied using finite element methods [28–32], finite difference algorithms [33–40], spectral methods [41,42], and collocation techniques [43,44] based on Legendre and Chebyshev polynomials [45]. Recently, Dehghan and Mirzaei [46] applied a numerical method based on the boundary integral equation and dual reciprocity methods using radial basis functions [47,48].

The governing equations for two incompressible and immiscible fluids are the Navier–Stokes–Cahn–Hilliard equations [49–64]:

$$\rho(\phi) \left( \frac{\partial \mathbf{u}}{\partial t} + \mathbf{u} \cdot \nabla \mathbf{u} \right) = -\nabla p + \frac{1}{Re} \Delta \mathbf{u} + \frac{\rho(\phi)}{Fr^2} \mathbf{g}, \tag{1}$$

$$\nabla \cdot \mathbf{u} = 0, \tag{2}$$

$$\frac{\partial \phi}{\partial t} + \nabla \cdot (\phi \mathbf{u}) = \frac{1}{Pe} \Delta \mu, \tag{3}$$

$$\mu = f(\phi) - \epsilon^2 \Delta \phi, \tag{4}$$

where  $\mathbf{u}$  is the velocity,  $p$  is the pressure,  $\rho(\phi) = (\rho_H(1 + \phi)/2 + \rho_L(1 - \phi)/2)\rho_c$  is the variable density,  $\mathbf{g} = (0, 0, -1)$  is the gravitational direction, and  $\mu$  is the generalized chemical potential.  $f(\phi) = \phi^3 - \phi$  and  $\epsilon$  are redefined according to the scaling. The dimensionless parameters are the Reynolds number,  $Re = \rho_c U_c L_c / \eta$ , the Froude number,  $Fr = U_c / \sqrt{g L_c}$ , and the Péclet number,  $Pe = U_c L_c / (M \mu_c)$ . Here, the subscript 'c' indicates characteristic values used to make the governing equations dimensionless,  $\eta$  is the viscosity,  $g$  is the gravitational acceleration, and  $M$  is the mobility. In this paper, the effect of the surface tension is neglected. We note that even though our phase-field method can deal with the variable viscosity case straightforwardly, we focus on the viscosity matched case. When the densities of two incompressible fluids are different, the incompressible condition (2) is no longer valid in the mixed region of the two incompressible fluids despite each fluid being incompressible. Such fluids are referred to as quasi-incompressible in Ref. [65]. In recent work [66], the authors discussed this issue and formulated a pair of phase-field models that conserve mass, momentum, and total volume for each individual phase of two fluids.

This paper is organized as follows. In Section 2, we give a numerical solution with linear and nonlinear multigrid methods [67,68]. The pressure boundary condition which allows long time simulation will also be addressed in this section. Numerical results for the three-dimensional RTI are presented in Section 3. In Section 4, conclusions are drawn.

## 2. A numerical solution

The solution of large systems of equations resulting from discretization of the governing equations (1)–(4) is very costly, especially in three dimensions. An efficient approximation can be obtained by decoupling the solution of the momentum equations from the solution of the continuity equation by a projection method [69–74].

Let a three-dimensional computational domain be partitioned in Cartesian geometry into a uniform mesh with mesh spacing  $h$ . The center of each cell,  $\Omega_{ijk}$ , is located at  $(x_i, y_j, z_k) = ((i - 0.5)h, (j - 0.5)h, (k - 0.5)h)$  for  $i = 1, \dots, N_x, j = 1, \dots, N_y$ , and  $k = 1, \dots, N_z$ .  $N_x, N_y$ , and  $N_z$  are the numbers of cells in the  $x$ -,  $y$ -, and  $z$ -directions, respectively. Cell vertices are located at  $(x_{i+\frac{1}{2}}, y_{j+\frac{1}{2}}, z_{k+\frac{1}{2}}) = (ih, jh, kh)$ . In this paper, the fluid variables are defined on a staggered marker-and-cell (MAC) mesh introduced by Harlow and Welch [75]; that is, pressures and phase fields are stored at cell centers and velocities at cell faces (see Fig. 1).

Let  $\Delta t$  be the time step and  $n$  be the time step index. At the beginning of each time step, given  $\mathbf{u}^n$  and  $\phi^n$ , we want to find  $\mathbf{u}^{n+1}$ ,  $p^{n+1}$ , and  $\phi^{n+1}$  which solve the following temporal discretization of Eqs. (1)–(4):

$$\rho^n \frac{\mathbf{u}^{n+1} - \mathbf{u}^n}{\Delta t} = -\rho^n (\mathbf{u} \cdot \nabla \mathbf{u})^n - \nabla_d p^{n+1} + \frac{1}{Re} \Delta_d \mathbf{u}^n + \frac{\rho^n}{Fr^2} \mathbf{g},$$

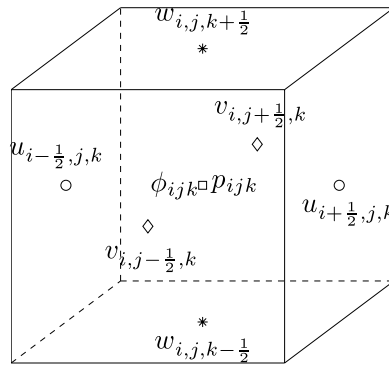


**Fig. 1.** Location of the fluid variables on a MAC mesh cell. Velocities are defined at the cell faces while pressures and phase fields are defined at the cell centers.

$$\nabla_d \cdot \mathbf{u}^{n+1} = 0,$$

$$\frac{\phi^{n+1} - \phi^n}{\Delta t} = -\nabla_d \cdot (\phi \mathbf{u})^n + \frac{1}{Pe} \Delta_d v^{n+1} - \frac{1}{Pe} \Delta_d \phi^n, \tag{5}$$

$$v^{n+1} = (\phi^{n+1})^3 - \epsilon^2 \Delta_d \phi^{n+1}, \tag{6}$$

where  $\rho^n = \rho(\phi^n)$ . The outline of the main procedures in one time step is as follows.

*Step 1.* Initialize  $\phi^0$  to be the locally equilibrated composition profile and  $\mathbf{u}^0$  to be the divergence-free velocity field.

*Step 2.* Solve for an intermediate velocity field,  $\tilde{\mathbf{u}}$ , which generally does not satisfy the continuity equation, without the pressure gradient:

$$\frac{\tilde{\mathbf{u}} - \mathbf{u}^n}{\Delta t} = -(\mathbf{u} \cdot \nabla_d \mathbf{u})^n + \frac{1}{\rho^n Re} \Delta_d \mathbf{u}^n + \frac{1}{Fr^2} \mathbf{g},$$

where the convective term,  $(\mathbf{u} \cdot \nabla_d \mathbf{u})^n$ , is computed using an upwind scheme [62,63].

Then, we solve the following equations for the advanced pressure field at the  $(n + 1)$ th time step:

$$\frac{\mathbf{u}^{n+1} - \tilde{\mathbf{u}}}{\Delta t} = -\frac{1}{\rho^n} \nabla_d p^{n+1}, \tag{7}$$

$$\nabla_d \cdot \mathbf{u}^{n+1} = 0. \tag{8}$$

Applying the divergence operator to Eq. (7), we find that Eq. (7) is equivalent to a Poisson equation for  $p^{n+1}$ :

$$\nabla_d \cdot \left( \frac{1}{\rho^n} \nabla_d p^{n+1} \right) = \frac{1}{\Delta t} \nabla_d \cdot \tilde{\mathbf{u}}, \tag{9}$$

where we have made use of Eq. (8) and the terms are defined as follows:

$$\begin{aligned} \nabla_d \cdot \left( \frac{1}{\rho^n} \nabla_d p_{ijk}^{n+1} \right) &= \frac{\frac{1}{\rho^n} p_{i+1,j,k}^{n+1} + \frac{1}{\rho^n} p_{i-1,j,k}^{n+1} + \frac{1}{\rho^n} p_{i,j+1,k}^{n+1} + \frac{1}{\rho^n} p_{i,j-1,k}^{n+1}}{h^2} \\ &\quad + \frac{\frac{1}{\rho^n} p_{i,j,k+\frac{1}{2}}^{n+1} + \frac{1}{\rho^n} p_{i,j,k-\frac{1}{2}}^{n+1}}{h^2} \\ &\quad - \frac{\frac{1}{\rho^n} \frac{1}{i+\frac{1}{2},j,k} + \frac{1}{\rho^n} \frac{1}{i-\frac{1}{2},j,k} + \frac{1}{\rho^n} \frac{1}{i,j+\frac{1}{2},k} + \frac{1}{\rho^n} \frac{1}{i,j-\frac{1}{2},k} + \frac{1}{\rho^n} \frac{1}{i,j,k+\frac{1}{2}} + \frac{1}{\rho^n} \frac{1}{i,j,k-\frac{1}{2}}}{h^2} p_{ijk}^{n+1}, \\ \nabla_d \cdot \tilde{\mathbf{u}}_{ijk} &= \frac{\tilde{u}_{i+\frac{1}{2},j,k} - \tilde{u}_{i-\frac{1}{2},j,k}}{h} + \frac{\tilde{v}_{i,j+\frac{1}{2},k} - \tilde{v}_{i,j-\frac{1}{2},k}}{h} + \frac{\tilde{w}_{i,j,k+\frac{1}{2}} - \tilde{w}_{i,j,k-\frac{1}{2}}}{h}, \end{aligned}$$

where  $\rho^n_{i+\frac{1}{2},j,k} = (\rho^n_{i+1,j,k} + \rho^n_{ijk})/2$  and the other terms are similarly defined.

The boundary condition for the pressure [62] is

$$\mathbf{n} \cdot \nabla_d p^{n+1} = \mathbf{n} \cdot \left( -\rho^n \frac{\mathbf{u}^{n+1} - \mathbf{u}^n}{\Delta t} - \rho^n (\mathbf{u} \cdot \nabla_d \mathbf{u})^n + \frac{1}{Re} \Delta_d \mathbf{u}^n + \frac{\rho^n}{Fr^2} \mathbf{g} \right),$$

where  $\mathbf{n}$  is the unit vector normal to the domain boundary.

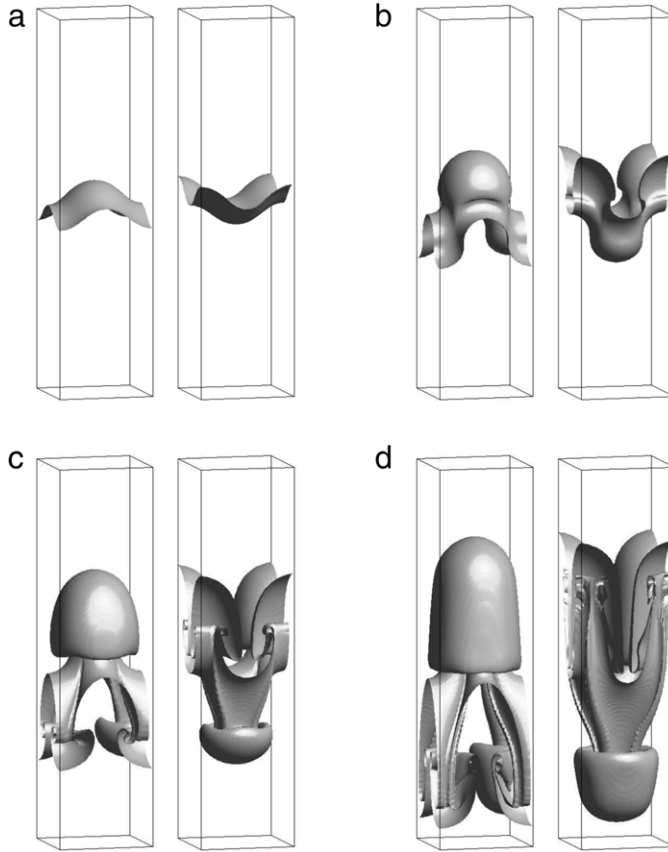


**Fig. 2.** Evolution of the interface at (a)  $t = 1.0$ , (b)  $t = 2.0$ , (c)  $t = 3.0$ , and (d)  $t = 4.0$ . The Atwood number is 0.5 and the Reynolds number is 1024. The interface is viewed from the heavy-fluid side (left column) and from the light-fluid side (right column). The interfaces in the left column are shifted 0.5 in both  $x$ - and  $y$ -directions for a better view of the bubble.

In our application of the phase-field method to the three-dimensional RTI, we will use periodic boundary conditions at the four sides and no slip boundary conditions at the top and bottom walls. Therefore,

$$\mathbf{n} \cdot \nabla_d p^{n+1} = \mathbf{n} \cdot \frac{\rho^n}{Fr^2} \mathbf{g}, \quad \text{i.e., } \frac{\partial p^{n+1}}{\partial z} = -\frac{\rho^n}{Fr^2} \text{ at } z = 0 \text{ and } z = L_z.$$

The resulting linear system of Eq. (9) is solved by a fast solver, such as a linear multigrid method [67]. Also, a Gauss–Seidel relaxation scheme is used as the smoother in the multigrid method. Then, the divergence-free velocities are defined by

$$\mathbf{u}^{n+1} = \tilde{\mathbf{u}} - \frac{\Delta t}{\rho^n} \nabla_d p^{n+1}.$$

*Step 3.* Update the phase field  $\phi^n$  to  $\phi^{n+1}$ . We implement an unconditionally gradient stable scheme in Eqs. (5) and (6) with a nonlinear multigrid method [67]. For a detailed description of the numerical method used in solving Eqs. (5) and (6), please refer to Refs. [38,76].

Since we are interested in a long time simulation, mass conservation is an important factor. Therefore, we use a conservative discretization of the convective part of the phase field Eq. (5):

$$\begin{aligned} ((\phi u)_x + (\phi v)_y + (\phi w)_z)_{ijk}^n &= \frac{u_{i+\frac{1}{2},j,k}^n (\phi_{i+1,j,k}^n + \phi_{ijk}^n) - u_{i-\frac{1}{2},j,k}^n (\phi_{ijk}^n + \phi_{i-1,j,k}^n)}{2h} \\ &+ \frac{v_{i,j+\frac{1}{2},k}^n (\phi_{i,j+1,k}^n + \phi_{ijk}^n) - v_{i,j-\frac{1}{2},k}^n (\phi_{ijk}^n + \phi_{i,j-1,k}^n)}{2h} \\ &+ \frac{w_{i,j,k+\frac{1}{2}}^n (\phi_{i,j,k+1}^n + \phi_{ijk}^n) - w_{i,j,k-\frac{1}{2}}^n (\phi_{ijk}^n + \phi_{i,j,k-1}^n)}{2h}. \end{aligned}$$

These complete one time step.

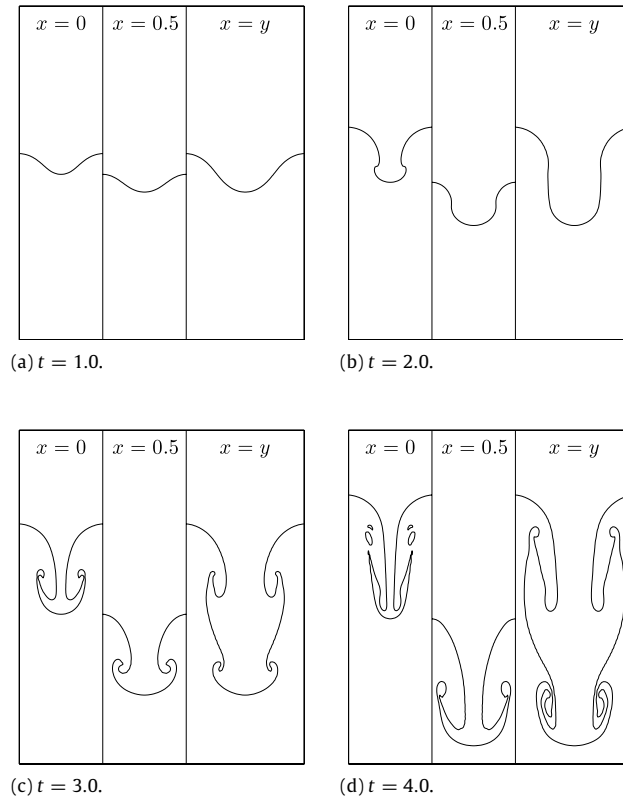


Fig. 3. Cross-sectional views of the interface at three vertical planes,  $x = 0$ ,  $x = 0.5$ , and  $x = y$ . Times are shown below each figure.

### 3. Numerical results

In this section, we simulate the three-dimensional RTI in a rectangular box with a square horizontal cross-section. In the previous work of He et al. [22], similar numerical experiments were performed using a lattice Boltzmann method. The height–width aspect ratio is fixed at 4:1. Unless otherwise specified, the initial condition is

$$\phi(x, y, z, 0) = \tanh\left(\frac{z - 2 - 0.05(\cos(2\pi x) + \cos(2\pi y))}{\sqrt{2}\epsilon}\right)$$

on the computational domain  $\Omega = (0, 1) \times (0, 1) \times (0, 4)$ .

#### 3.1. Three-dimensional Rayleigh–Taylor instability

The evolution of the interface in the three-dimensional RTI is shown in Fig. 2. Left and right columns in each subfigure show two different views of the interface from the heavy-fluid side and the light-fluid side, respectively. Here, the Atwood number is 0.5 and the Reynolds number is 1024. And we use  $h = 1/128$  (a  $128 \times 128 \times 512$  grid),  $\Delta t = 0.001$ ,  $\epsilon = 0.01$ , and  $Pe = 100/\epsilon$ . During the early stages, the interface grows nearly symmetrically up and down and remains rather simple (see Fig. 2(a)). But, as time goes by, it becomes more complicated and spikes of the heavy fluid first form near the middle of the four sides of the computational domain (see Fig. 2(b)). The roll-up at the edge of the spike starts at a later time (see Fig. 2(c)). At  $t = 4.0$ , these roll-ups are stretched into two extra layers of the heavy fluid folded upward (see Fig. 2(d)). This two-layer roll-up phenomenon is a unique feature of the three-dimensional RTI. Fig. 3 shows cross-sectional views of the interface at three vertical planes,  $x = 0$ ,  $x = 0.5$ , and  $x = y$ . The interfaces in the  $x = 0$  and  $x = 0.5$  planes look like those in the two-dimensional RTI. However, the interface in the  $x = y$  plane is quite different. In this plane, we can see clearly the two-layer roll-up phenomenon. These results are in qualitative agreement with the previous computations of Li et al. [21] and He et al. [22].

#### 3.2. Long time evolution of the three-dimensional Rayleigh–Taylor instability

Owing to the pressure boundary treatment mentioned in Section 2, we can perform long time evolution resulting in an equilibrium state. The Atwood number is 0.5 and the Reynolds number is 3000. And we use  $h = 1/64$  (a  $64 \times 64 \times 256$

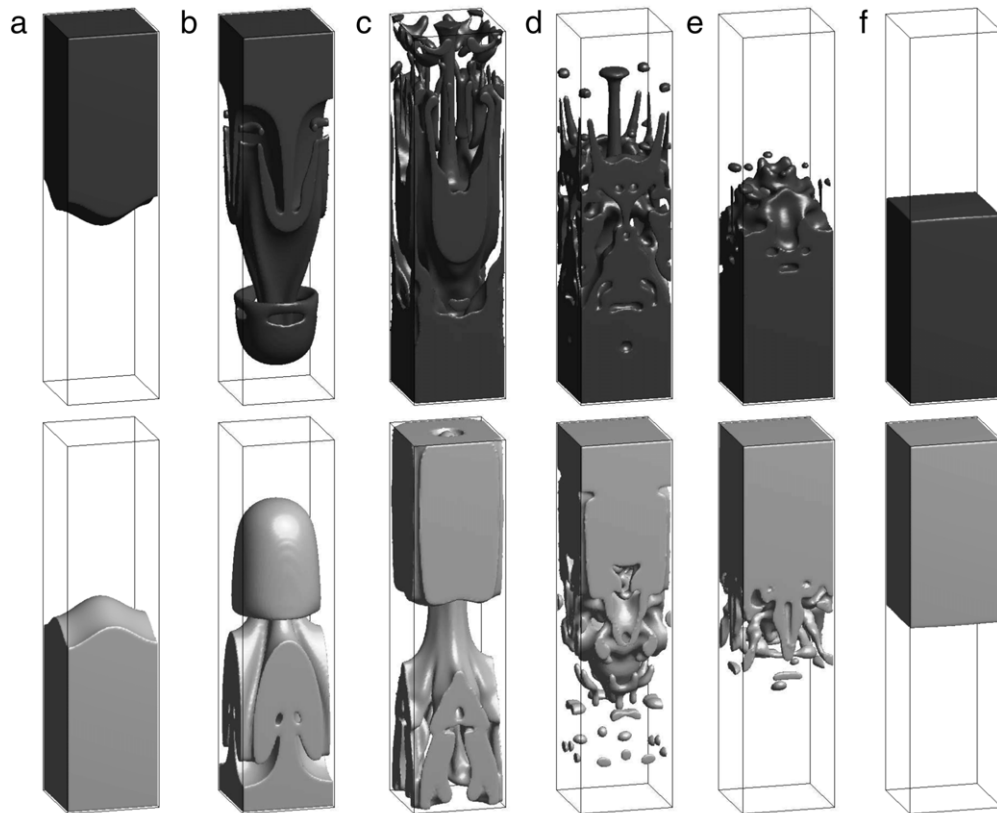


**Fig. 4.** Long time evolution of the three-dimensional Rayleigh–Taylor instability at (a)  $t = 0$ , (b)  $t = 3.53$ , (c)  $t = 7.07$ , (d)  $t = 14.14$ , (e)  $t = 17.67$ , and (f)  $t = 70.7$ . Top and bottom rows show two different views of the interface from the light-fluid side and the heavy-fluid side, respectively.

grid),  $\Delta t = 0.001\sqrt{2}$ ,  $\epsilon = 0.01\sqrt{2}$ , and  $Pe = 1/\epsilon$ . The evolution of the interface is shown in Fig. 4. At time  $t = 70.7$ , the heavy fluid falls down and the light fluid rises up completely.

### 3.3. The effect of the Reynolds number

To investigate the effect of the Reynolds number on the three-dimensional RTI, we perform numerical simulations at a number of Reynolds numbers with the Atwood number fixed at 0.5. We use  $h = 1/128$  (a  $128 \times 128 \times 512$  grid),  $\Delta t = 0.001$ ,  $\epsilon = 0.01$ , and  $Pe = 1/\epsilon$ . Fig. 5 shows the positions of the bubble front, spike tip, and saddle point at different Reynolds numbers. For all Reynolds numbers, at later times, the bubble rises with a constant speed and the spike accelerates slightly. The saddle points move downward as time increases, but the movement is rather slow compared to those of the bubble and spike. Also, we observe that a decrease in the Reynolds number delays the development of the RTI. This delay is larger for the spike than for the bubble and saddle points. The effect of the Reynolds number is obvious at low Reynolds numbers but becomes negligible for  $Re > 512$ .

### 3.4. The effect of the Atwood number

To study the effect of the Atwood number on the three-dimensional RTI, we perform numerical simulations at a number of Atwood numbers with the Reynolds number fixed at 1024. We use  $h = 1/128$  (a  $128 \times 128 \times 512$  grid),  $\Delta t = 0.001$ ,  $\epsilon = 0.01$ , and  $Pe = 1/\epsilon$ . Fig. 6 shows the positions of the bubble front, spike tip, and saddle point at different Atwood numbers. When the Atwood number is small (at  $At = 0.2$ ), the position change of the bubble front is almost the same as that of the spike tip. This means that the interface grows nearly symmetrically up and down. However, as the Atwood number increases, the position of the spike tip changes much more quickly than that of the bubble front and the symmetry of the initial structure becomes lost. From the results of Fig. 6, we see that the three-dimensional RTI exhibits a strong dependence on the Atwood number.

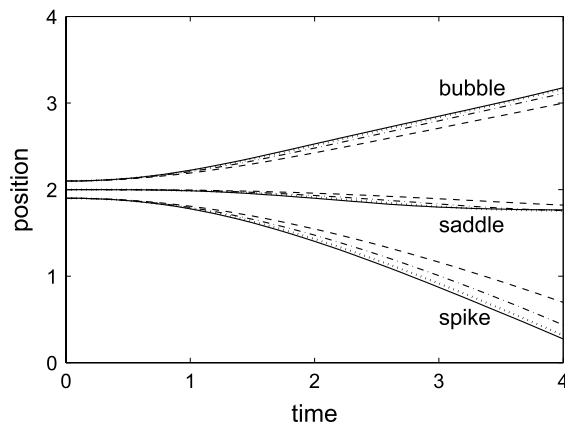


**Fig. 5.** Effect of the Reynolds number on the positions of the bubble front, spike tip, and saddle point. The Atwood number is fixed at 0.5. Solid, dotted, dash-dotted, and dashed lines show the results for  $Re = 1024, 512, 256,$  and  $128,$  respectively.

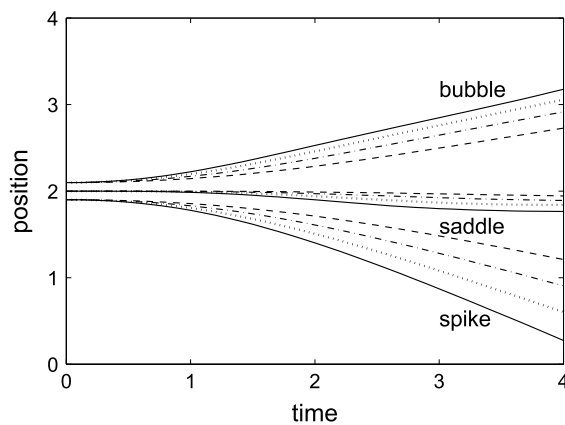


**Fig. 6.** Effect of the Atwood number on the positions of the bubble front, spike tip, and saddle point. The Reynolds number is fixed at 1024. Solid, dotted, dash-dotted, and dashed lines are the results of  $At = 0.5, 0.4, 0.3,$  and  $0.2,$  respectively.

#### 4. Conclusions

The three-dimensional RTI between two incompressible and immiscible fluids was studied using a phase field. During the early stages, the interface grows nearly symmetrically up and down and remains rather simple. During the late stages, the heavy fluid rolls up at both the saddle point and the spike tip due to the Kelvin–Helmholtz instability. As a result, we observed the two-layer roll-up phenomenon of the heavy fluid, which does not occur in the two-dimensional case. And we studied the positions of the bubble front, spike tip, and saddle point to investigate the effect of the Reynolds and Atwood numbers on the three-dimensional RTI. We showed that a decrease in the Reynolds or Atwood numbers delays the development of the RTI. Note that the three-dimensional RTI exhibits a stronger dependence on the Atwood number than on the Reynolds number. Finally, owing to the pressure boundary treatment, we were able to perform long time three-dimensional simulation resulting in an equilibrium state.

#### Acknowledgments

The first author (Hyun Geun Lee) was supported by Basic Science Research Program through the National Research Foundation of Korea (NRF) funded by the Ministry of Education (2009-0093827, 2012R1A6A3A01019827). The corresponding author (J.S. Kim) thanks the reviewers for their constructive comments and suggestions.

#### References

- [1] L. Rayleigh, Investigation of the character of the equilibrium of an incompressible heavy fluid of variable density, *Proc. Lond. Math. Soc.* 14 (1883) 170–177.
- [2] G. Taylor, The instability of liquid surfaces when accelerated in a direction perpendicular to their planes. I, *Proc. R. Soc. Lond. Ser. A* 201 (1950) 192–196.
- [3] J.D. Lindl, R.L. McCrory, E.M. Campbell, Progress toward ignition and burn propagation in inertial confinement fusion, *Phys. Today* 45 (1992) 32–40.

- [4] J.D. Kilkenny, S.G. Glendinning, S.W. Haan, B.A. Hammel, J.D. Lindl, D. Munro, B.A. Remington, S.V. Weber, J.P. Knauer, C.P. Verdon, A review of the ablative stabilization of the Rayleigh–Taylor instability in regimes relevant to inertial confinement fusion, *Phys. Plasmas* 1 (1994) 1379–1389.
- [5] J. Lindl, Development of the indirect-drive approach to inertial confinement fusion and the target physics basis for ignition and gain, *Phys. Plasmas* 2 (1995) 3933–4024.
- [6] R. Betti, V.N. Goncharov, R.L. McCrory, C.P. Verdon, Growth rates of the ablative Rayleigh–Taylor instability in inertial confinement fusion, *Phys. Plasmas* 5 (1998) 1446–1454.
- [7] M. Livio, J.R. Buchler, S.A. Colgate, Rayleigh–Taylor driven supernova explosions: a two-dimensional numerical study, *Astrophys. J.* 238 (1980) L139–L143.
- [8] S. Yamada, K. Sato, Rayleigh–Taylor instability in the asymmetric supernova explosion, *Astrophys. J.* 382 (1991) 594–602.
- [9] J.M. Blondin, D.C. Ellison, Rayleigh–Taylor instabilities in young supernova remnants undergoing efficient particle acceleration, *Astrophys. J.* 560 (2001) 244–253.
- [10] X. Ribeyre, V.T. Tikhonchuk, S. Bouquet, Compressible Rayleigh–Taylor instabilities in supernova remnants, *Phys. Fluids* 16 (2004) 4661–4670.
- [11] M.J. Keskinen, E.P. Szuszczewicz, S.L. Ossakow, J.C. Holmes, Nonlinear theory and experimental observations of the local collisional Rayleigh–Taylor instability in a descending equatorial spread F ionosphere, *J. Geophys. Res.* 86 (1981) 5785–5792.
- [12] H.-P. Plag, H.-U. Jüttner, Rayleigh–Taylor instabilities of a self-gravitating earth, *J. Geodynamics* 20 (1995) 267–288.
- [13] L. Debnath, *Nonlinear Water Waves*, Academic Press, Boston, 1994.
- [14] D.H. Sharp, An overview of Rayleigh–Taylor instability, *Physica D* 12 (1984) 3–18.
- [15] S. Chandrasekhar, *Hydrodynamic and Hydromagnetic Stability*, Oxford University Press, Oxford, 1961.
- [16] G. Tryggvason, S.O. Unverdi, Computations of three-dimensional Rayleigh–Taylor instability, *Phys. Fluids A* 2 (1990) 656–659.
- [17] T. Yabe, H. Hoshino, T. Tsuchiya, Two- and three-dimensional behavior of Rayleigh–Taylor and Kelvin–Helmholtz instabilities, *Phys. Rev. A* 44 (1991) 2756–2758.
- [18] D.L. Youngs, Three-dimensional numerical simulation of turbulent mixing by Rayleigh–Taylor instability, *Phys. Fluids A* 3 (1991) 1312–1320.
- [19] X.L. Li, Study of three-dimensional Rayleigh–Taylor instability in compressible fluids through level set method and parallel computation, *Phys. Fluids A* 5 (1993) 1904–1913.
- [20] J. Hecht, D. Ofer, U. Alon, D. Shvarts, S.A. Orszag, D. Shvarts, R.L. McCrory, Three-dimensional simulations and analysis of the nonlinear stage of the Rayleigh–Taylor instability, *Laser Part. Beams* 13 (1995) 423–440.
- [21] X.L. Li, B.X. Jin, J. Glimm, Numerical study for the three-dimensional Rayleigh–Taylor instability through the TVD/AC scheme and parallel computation, *J. Comput. Phys.* 126 (1996) 343–355.
- [22] X. He, R. Zhang, S. Chen, G.D. Doolen, On the three-dimensional Rayleigh–Taylor instability, *Phys. Fluids* 11 (1999) 1143–1152.
- [23] J. Glimm, J.W. Grove, X.L. Li, D.C. Tan, Robust computational algorithms for dynamic interface tracking in three dimensions, *SIAM J. Sci. Comput.* 21 (2000) 2240–2256.
- [24] Y.-N. Young, H. Tufo, A. Dubey, R. Rosner, On the miscible Rayleigh–Taylor instability: two and three dimensions, *J. Fluid Mech.* 447 (2001) 377–408.
- [25] G. Dimonte, D.L. Youngs, A. Dimits, S. Weber, M. Marinak, S. Wunsch, C. Garasi, A. Robinson, M.J. Andrews, P. Ramaprabhu, A.C. Calder, B. Fryxell, J. Biello, L. Dursi, P. MacNeice, K. Olson, P. Ricker, R. Rosner, F. Timmes, H. Tufo, Y.-N. Young, M. Zingale, A comparative study of the turbulent Rayleigh–Taylor instability using high-resolution three-dimensional numerical simulations: the alpha-group collaboration, *Phys. Fluids* 16 (2004) 1668–1693.
- [26] A.E. Deane, Parallel computations of 3-D Rayleigh–Taylor instability, *Comput. Math. Appl.* 35 (1998) 111–116.
- [27] J.W. Cahn, J.E. Hilliard, Free energy of a nonuniform system. I. Interfacial free energy, *J. Chem. Phys.* 28 (1958) 258–267.
- [28] C.M. Elliott, D.A. French, A nonconforming finite-element method for the two-dimensional Cahn–Hilliard equation, *SIAM J. Numer. Anal.* 26 (1989) 884–903.
- [29] C.M. Elliott, D.A. French, F.A. Milner, A second order splitting method for the Cahn–Hilliard equation, *Numer. Math.* 54 (1989) 575–590.
- [30] C.M. Elliott, S. Larsson, Error estimates with smooth and nonsmooth data for a finite element method for the Cahn–Hilliard equation, *Math. Comp.* 58 (1992) 603–630.
- [31] J.W. Barrett, J.F. Blowey, Finite element approximation of the Cahn–Hilliard equation with concentration dependent mobility, *Math. Comp.* 68 (1999) 487–517.
- [32] D. Kay, R. Welford, A multigrid finite element solver for the Cahn–Hilliard equation, *J. Comput. Phys.* 212 (2006) 288–304.
- [33] S.M. Choo, S.K. Chung, Conservative nonlinear difference scheme for the Cahn–Hilliard equation, *Comput. Math. Appl.* 36 (1998) 31–39.
- [34] S.M. Choo, S.K. Chung, K.I. Kim, Conservative nonlinear difference scheme for the Cahn–Hilliard equation—II, *Comput. Math. Appl.* 39 (2000) 229–243.
- [35] D. Furihata, A stable and conservative finite difference scheme for the Cahn–Hilliard equation, *Numer. Math.* 87 (2001) 675–699.
- [36] J. Kim, K. Kang, J. Lowengrub, Conservative multigrid methods for Cahn–Hilliard fluids, *J. Comput. Phys.* 193 (2004) 511–543.
- [37] E.V.L. de Mello, O.T. da Silveira Filho, Numerical study of the Cahn–Hilliard equation in one, two and three dimensions, *Physica A* 347 (2005) 429–443.
- [38] J. Kim, A numerical method for the Cahn–Hilliard equation with a variable mobility, *Commun. Nonlinear Sci. Numer. Simul.* 12 (2007) 1560–1571.
- [39] H.G. Lee, J. Kim, A second-order accurate non-linear difference scheme for the  $N$ -component Cahn–Hilliard system, *Physica A* 387 (2008) 4787–4799.
- [40] H.G. Lee, J.-W. Choi, J. Kim, A practically unconditionally gradient stable scheme for the  $N$ -component Cahn–Hilliard system, *Physica A* 391 (2012) 1009–1019.
- [41] X. Ye, X. Cheng, The Fourier spectral method for the Cahn–Hilliard equation, *Appl. Math. Comput.* 171 (2005) 345–357.
- [42] Y. He, Y. Liu, T. Tang, On large time-stepping methods for the Cahn–Hilliard equation, *Appl. Numer. Math.* 57 (2007) 616–628.
- [43] X. Ye, The Legendre collocation method for the Cahn–Hilliard equation, *J. Comput. Appl. Math.* 150 (2003) 87–108.
- [44] S. Emmanuel, A. Cortis, B. Berkowitz, Diffusion in multicomponent systems: a free energy approach, *Chem. Phys.* 302 (2004) 21–30.
- [45] M. Lakestani, M. Dehghan, Numerical solution of Riccati equation using the cubic  $B$ -spline scaling functions and Chebyshev cardinal functions, *Comput. Phys. Comm.* 181 (2010) 957–966.
- [46] M. Dehghan, D. Mirzaei, A numerical method based on the boundary integral equation and dual reciprocity methods for one-dimensional Cahn–Hilliard equation, *Eng. Anal. Bound. Elem.* 33 (2009) 522–528.
- [47] M. Dehghan, A. Shokri, A numerical method for solution of the two-dimensional sine–Gordon equation using the radial basis functions, *Math. Comput. Simul.* 79 (2008) 700–715.
- [48] M. Dehghan, A. Shokri, Numerical solution of the nonlinear Klein–Gordon equation using radial basis functions, *J. Comput. Appl. Math.* 230 (2009) 400–410.
- [49] R. Chella, J. Viñals, Mixing of a two-phase fluid by cavity flow, *Phys. Rev. E* 53 (1996) 3832–3840.
- [50] D. Jacqmin, Calculation of two-phase Navier–Stokes flows using phase-field modeling, *J. Comput. Phys.* 155 (1999) 96–127.
- [51] D. Jacqmin, Contact-line dynamics of a diffuse fluid interface, *J. Fluid Mech.* 402 (2000) 57–88.
- [52] V.E. Badalassi, H.D. Ceniceros, S. Banerjee, Computation of multiphase systems with phase field models, *J. Comput. Phys.* 190 (2003) 371–397.
- [53] C. Liu, J. Shen, A phase field model for the mixture of two incompressible fluids and its approximation by a Fourier-spectral method, *Physica D* 179 (2003) 211–228.
- [54] P. Yue, J.J. Feng, C. Liu, J. Shen, A diffuse-interface method for simulating two-phase flows of complex fluids, *J. Fluid Mech.* 515 (2004) 293–317.
- [55] J. Kim, A continuous surface tension force formulation for diffuse-interface models, *J. Comput. Phys.* 204 (2005) 784–804.
- [56] J. Kim, J. Lowengrub, Phase field modeling and simulation of three-phase flows, *Interfaces Free Bound.* 7 (2005) 435–466.
- [57] F. Boyer, C. Lapuerta, Study of a three component Cahn–Hilliard flow model, *ESAIM Math. Model. Numer. Anal.* 40 (2006) 653–687.
- [58] H. Ding, P.D.M. Spelt, C. Shu, Diffuse interface model for incompressible two-phase flows with large density ratios, *J. Comput. Phys.* 226 (2007) 2078–2095.
- [59] A. Celani, A. Mazzino, P. Muratore-Ginanneschi, L. Vozella, Phase-field model for the Rayleigh–Taylor instability of immiscible fluids, *J. Fluid Mech.* 622 (2009) 115–134.

- [60] J. Kim, A generalized continuous surface tension force formulation for phase-field models for multi-component immiscible fluid flows, *Comput. Methods Appl. Mech. Engrg.* 198 (2009) 3105–3112.
- [61] C.-H. Kim, S.-H. Shin, H.G. Lee, J. Kim, Phase-field model for the pinchoff of liquid–liquid jets, *J. Korean Phys. Soc.* 55 (2009) 1451–1460.
- [62] H.G. Lee, K.M. Kim, J. Kim, On the long time simulation of the Rayleigh–Taylor instability, *Internat. J. Numer. Methods Engrg.* 85 (2011) 1633–1647.
- [63] H.G. Lee, J. Kim, A comparison study of the Boussinesq and the variable density models on buoyancy-driven flows, *J. Eng. Math.* 75 (2012) 15–27.
- [64] O. Axelsson, P. Boyanova, M. Kronbichler, M. Neytcheva, X. Wu, Numerical and computational efficiency of solvers for two-phase problems, *Comput. Math. Appl.* 65 (2013) 301–314.
- [65] J. Lowengrub, L. Truskinovsky, Quasi-incompressible Cahn–Hilliard fluids and topological transitions, *Proc. R. Soc. Lond. Ser. A* 454 (1998) 2617–2654.
- [66] J. Shen, X. Yang, Q. Wang, Mass and volume conservation in phase field models for binary fluids, *Commun. Comput. Phys.* 13 (2013) 1045–1065.
- [67] U. Trottenberg, C. Oosterlee, A. Schüller, *Multigrid*, Academic press, London, 2001.
- [68] M. Dehghan, A. Mohebbi, Multigrid solution of high order discretisation for three-dimensional biharmonic equation with Dirichlet boundary conditions of second kind, *Appl. Math. Comput.* 180 (2006) 575–593.
- [69] A.J. Chorin, A numerical method for solving incompressible viscous flow problems, *J. Comput. Phys.* 2 (1967) 12–26.
- [70] J.B. Bell, P. Colella, H.M. Glaz, A second-order projection method for the incompressible Navier–Stokes equations, *J. Comput. Phys.* 85 (1989) 257–283.
- [71] R.S. Bernard, A MacCormack scheme for incompressible flow, *Comput. Math. Appl.* 24 (1992) 151–168.
- [72] J. Li, Y. Renardy, Numerical study of flows of two immiscible liquids at low Reynolds number, *SIAM Rev.* 42 (2000) 417–439.
- [73] W.B. Yang, H.Q. Zhang, C.K. Chan, W.Y. Lin, Large eddy simulation of mixing layer, *J. Comput. Appl. Math.* 163 (2004) 311–318.
- [74] H.-C. Lee, Y. Choi, Analysis and approximation of linear feedback control problems for the Boussinesq equations, *Comput. Math. Appl.* 51 (2006) 829–848.
- [75] F.H. Harlow, J.E. Welch, Numerical calculation of time-dependent viscous incompressible flow of fluid with free surface, *Phys. Fluids* 8 (1965) 2182–2189.
- [76] J. Kim, H.-O. Bae, An unconditionally stable adaptive mesh refinement for Cahn–Hilliard equation, *J. Korean Phys. Soc.* 53 (2008) 672–679.